Directed evolution of a far-red fluorescent rhodopsin

R. Scott McIsaac[a,1], Martin K. M. Engqvist[a,1], Timothy Wannier[b], Adam Z. Rosenthal[b], Lukas Herwig[a], Nicholas C. Flytzanis[b], Eleonora S. Imasheva[c], Janos K. Lanyi[c], Sergei P. Balashov[c], Viviana Gradinaru[b], and Frances H. Arnold[a,b,2]

Divisions of [a]Chemistry and Chemical Engineering and [b]Biology and Biological Engineering, California Institute of Technology, Pasadena, CA, 91125; and [c]Department of Physiology and Biophysics, University of California, Irvine School of Medicine, Irvine, CA 92697

Contributed by Frances H. Arnold, July 23, 2014 (sent for review June 19, 2014)

Microbial rhodopsins are a diverse group of photoactive transmembrane proteins found in all three domains of life. A member of this protein family, Archaerhodopsin-3 (Arch) of halobacterium *Halorubrum sodomense*, was recently shown to function as a fluorescent indicator of membrane potential when expressed in mammalian neurons. Arch fluorescence, however, is very dim and is not optimal for applications in live-cell imaging. We used directed evolution to identify mutations that dramatically improve the absolute brightness of Arch, as confirmed biochemically and with live-cell imaging (in *Escherichia coli* and human embryonic kidney 293 cells). In some fluorescent Arch variants, the pK_a of the protonated Schiff-base linkage to retinal is near neutral pH, a useful feature for voltage-sensing applications. These bright Arch variants enable labeling of biological membranes in the far-red/infrared and exhibit the furthest red-shifted fluorescence emission thus far reported for a fluorescent protein (maximal excitation/emission at ∼620 nm/730 nm).

optogenetics | opsins | bioelectricity | voltage sensor | near-infrared

Fluorescent proteins that emit at long (>650 nm) wavelengths are needed for applications in live-cell imaging. Mammalian tissues are most transparent to light in the near-infrared (NIR) window (650 nm–900 nm) due to the minimal absorption of water, melanin, and hemoglobin in this range (1). Microbial opsins are integral membrane proteins with seven transmembrane helices and a conserved lysine residue that forms a covalent Schiff-base linkage to *all-trans* retinal. The apoprotein covalently bonded to a retinal molecule forms a colored holoprotein referred to as rhodopsin (2), variants of which have recently been reported to naturally fluoresce at wavelengths >680 nm in live cells (3, 4). Rhodopsins thus offer novel substrates for engineering genetically encoded fluorescent markers in a desirable spectral range for live-cell imaging.

Microbial rhodopsins harvest light to facilitate adaptive responses (i.e., phototaxis) (5), generate proton gradients for converting solar energy into electrochemical energy (6, 7), and promote survival during starvation in marine bacteria (8). In the field of optogenetics, rhodopsins have been used as actuators of neuronal activity: When certain rhodopsin variants are expressed in neurons, light-driven ion flux can be exploited to activate (9) or inhibit (10) neuronal activity with fast kinetics in a selective and reversible fashion. The absorbance spectrum of rhodopsins can be sensitive to membrane voltage (11), and at least three rhodopsins have been reported to exhibit dim fluorescence that is sensitive to changes in membrane voltage (3, 4, 12), a property that has been harnessed to develop genetically encoded fluorescent sensors of neuronal activity (3, 12, 13). Although significant progress has been made in developing opsin-based tools that enable selective activation/inhibition of neurons, progress toward developing brighter opsin-based biological sensors has been limited. Brighter variants are essential for moving beyond single-cell imaging studies to studying populations of cells with wide-field imaging (13).

Archaerhodopsin-3 (Arch), a proton-pumping rhodopsin from the microbe *Halorubrum sodomense*, is reported to exhibit dim fluorescence that is sensitive to transmembrane voltage in the NIR range (3). This feature of Arch enables detection of voltage changes with submillisecond response times and optical monitoring of action potentials in cultured neurons (3). When proton-pumping activity is abolished by mutating residue D95, Arch fluorescence remains sensitive to transmembrane voltage (3). D95E is the only reported mutation at this residue to retain wild type-like kinetics of voltage-induced fluorescent changes (14). Currently, Arch and its variants have extremely low quantum efficiencies, which greatly limits their utility as voltage sensors and more generally as optical markers.

We recently used directed evolution to tune the absorption maximum (λ_{max}) of *Gloeobacter violaceus* rhodopsin (GR), shifting it by ±80 nm (15). We found that a subset of red-shifted GR variants exhibited increased levels of fluorescence in the far-red, demonstrating that rhodopsin fluorescence could be increased through mutations in the protein retinal-binding pocket to a greater extent than observed earlier for variants with protonated Schiff-base counter ion (16, 17). Although Arch and GR share only 26% amino acid sequence identity, we found that mutations from a bright GR variant can be transferred to the homologous positions in Arch to greatly improve its overall fluorescence (and red shift its λ_{max} by ∼70 nm). Given that directed evolution was effective at modifying GR spectral properties, we reasoned that it should also be useful in further improving Arch fluorescence. Through a combination of random and targeted site-saturation mutagenesis and accumulating beneficial mutations over multiple generations, we show that the absolute brightness of Arch can be increased >20-fold over that of the wild-type protein to create a fluorescent integral membrane protein useful for live-cell imaging and physiological sensing.

Significance

Archaerhodopsin-3 (Arch) is an integral membrane protein that can function as a genetically encoded fluorescent indicator of membrane voltage in neurons. The ability to visualize changes in membrane voltage is of great interest as a readout for neuronal activity. Published variants of this protein, however, are too dim to enable wide-field imaging of cell populations. We used directed evolution to increase the absolute brightness of Arch as a reporter for optogenetics research and live-cell imaging. This study establishes that introducing mutations around the retinal Schiff-base linkage and screening for increased fluorescence is an effective strategy for generating bright rhodopsin variants. At least some mutations discovered in one rhodopsin (*Gloeobacter violaceus* rhodopsin) can be transferred to another (Arch) to increase fluorescence.

Author contributions: R.S.M., M.K.M.E., and F.H.A. designed research; R.S.M., M.K.M.E., T.W., A.Z.R., L.H., N.C.F., E.S.I., and S.P.B. performed research; R.S.M., M.K.M.E., T.W., L.H., N.C.F., V.G., and F.H.A. contributed new reagents/analytic tools; R.S.M., M.K.M.E., T.W., A.Z.R., N.C.F., E.S.I., J.K.L., S.P.B., and F.H.A. analyzed data; and R.S.M. and F.H.A. wrote the paper.

The authors declare no conflict of interest.

[1]R.S.M. and M.K.M.E. contributed equally to this work.

[2]To whom correspondence should be addressed. Email: frances@cheme.caltech.edu.

This article contains supporting information online at www.pnas.org/lookup/suppl/doi:10.1073/pnas.1413987111/-/DCSupplemental.

Results

Transfer of GR Mutations to Arch Increases Arch Fluorescence. Although Arch and GR share low overall sequence identity, 16 of the 20 retinal binding pocket residues (defined as amino acids within 5 Å of retinal in Arch) are conserved between the two (Fig. S1). The mutations of a bright GR variant discovered in our previous directed evolution study of GR (15), GR(D121E/T125C/A256M), which contains the desirable D→E substitution at the Schiff-base counter ion, map to D95E, T99C, and A225M in Arch, respectively (Fig. S1). We recombined these mutations in Arch and identified two variants, Arch(D95E/T99C) (here referred to as Arch(DETC)) and Arch(D95E/T99C/A225M) (here referred to as Arch(DETCAM)), that exhibit large red shifts in λ_{max} compared with wild-type Arch (Fig. 1*A*) as well as an approximately fivefold increase in fluorescence in *Escherichia coli* at pH 6 (Fig. 1*B*). No other combinations of D95E, T99C, and A225M resulted in large changes in λ_{max} or improved fluorescence over wild-type Arch. Arch(DETC) and Arch(DETCAM) exhibited nearly identical levels of fluorescence (Fig. 1*B*). Because the A225M mutation did not further increase fluorescence in Arch(DETC), we chose to focus on Arch(DETC) for further characterization and engineering.

Directed Evolution of Arch(DETC) Further Increases Fluorescence. Although an initial mechanistic study of voltage-sensitive fluorescence in Arch was recently reported (18), it remained unclear which amino acid residues should be targeted for mutation to improve fluorescent properties [other than the Schiff-base counter ion, which is known to affect the lifetime of the fluorescence excited state in bacteriorhodopsin (16) and is already mutated in Arch(DETC)]. To identify mutations that increase Arch(DETC) fluorescence, we thus followed an unbiased approach by performing random mutagenesis over the whole protein (details in *Materials and Methods*) and screened 2,640 mutants in a 96-well plate assay at neutral pH (Fig. 2 and Fig. S2). Arch(DETC) was fused to cyan fluorescent protein (CFP) so that the overall expression level of each screened mutant could be monitored via CFP fluorescence. Separately, three mutations were identified (V59A, P60L, and P196S) that individually improve Arch(DETC) fluorescence by approximately two- to threefold at neutral pH

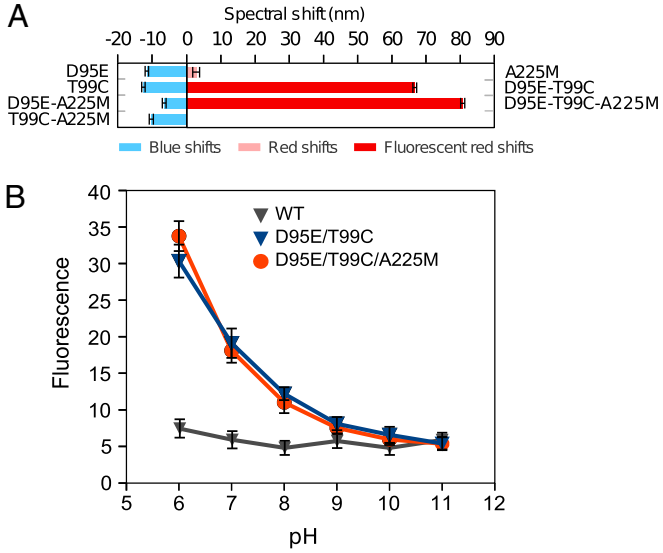

Fig. 1. Measuring the effects of mutations on Arch absorption maximum (λ_{max}) and fluorescence. (*A*) Quantifying the shift in λ_{max} between purified Arch and seven different mutants at pH 7.5. (*B*) Measuring the dependence of Arch, Arch(DETC), and Arch(DETCAM) fluorescence on pH.

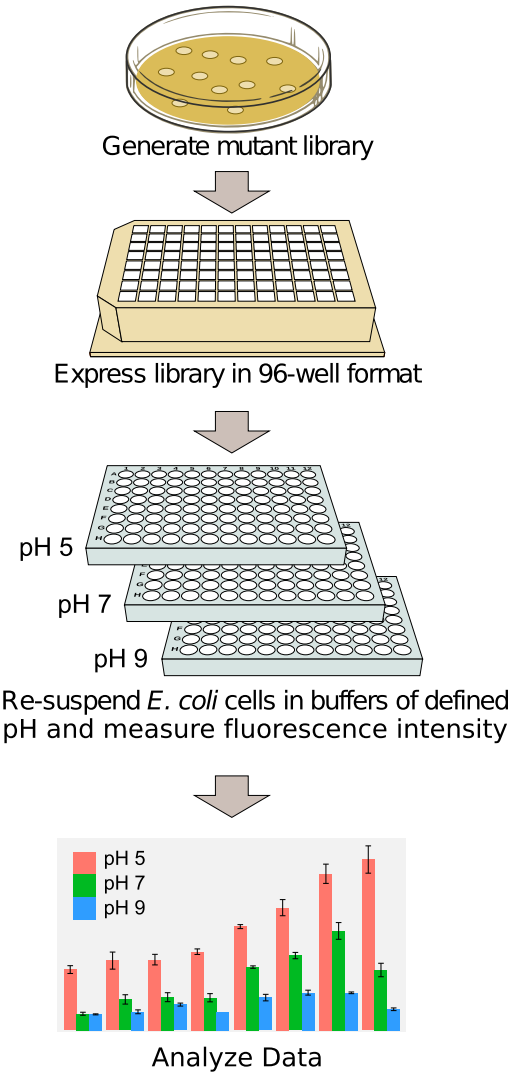

Fig. 2. Schematic of screening system for measuring fluorescence of Arch variants in 96-well format.

(Fig. 3). Two other mutations, I129T and I129V, also increased Arch(DETC) fluorescence, although to a lesser degree (Fig. 3). We validated the plate-based assay results by measuring Arch, Arch(DETC), and Arch(DETC+V59A) fluorescence with flow cytometry and also confirmed that they uniformly expressed in the *E. coli* population (Fig. S3). Although random mutagenesis allowed for mutations throughout the protein, all of the mutations that were identified to increase Arch(DETC) fluorescence were within 5 Å of retinal or the residue forming the Schiff base, K226 (based on a structural homology model between Arch and Archaerhodopsin-2, 86% amino acid identity) (Fig. 4). It thus appears that the most straightforward route to improving fluorescence in Arch is to mutate residues that are proximal to the retinal chromophore and especially the Schiff-base linkage.

Although error-prone PCR mutagenesis produces mutations throughout the protein, it does not enable access to all possible amino acid mutations at each position. We therefore decided to determine whether other amino acid substitutions further improve fluorescence over the V59A, P60L, and P196S variants by performing site-saturation mutagenesis at these three positions. We isolated many variants that showed slight increases in fluorescence over Arch(DETC), but none was substantially superior

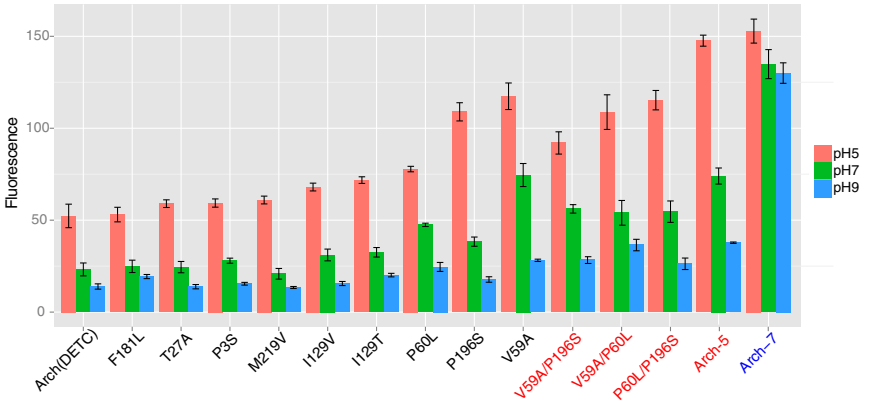

Fig. 3. Fluorescence of Arch variants measured in *E. coli* resuspended in phosphate buffer at pH 5, pH 7, and pH 9. All listed mutations are in the Arch(DETC) background. Individual mutations are written in black text (e.g., T27A refers to the Arch variant containing the mutations T27A, D95E, and T99C). Mutations of recombined variants from the initial error-prone PCR mutagenesis library are written in red text (e.g., V59A/P196S refers to the Arch variant containing the mutations V59A, D95E, T99C, and P196S). Arch-5 contains the mutations V59A, P60L, D95E, T99C, and P196S. Arch-7 contains the mutations V59A, P60L, D95E, T99C, P196S, D222S, and A225C.

to those identified by error-prone PCR mutagenesis and screening (Fig. S4 *A–C*).

To test whether the V59A, P60L, and P196S mutations could be combined to yield even higher fluorescence, the three possible double mutants and the triple mutant were constructed in the Arch(DETC) background (Fig. 3). Recombination of V59A, P60L, and P196S revealed that these mutations were not cumulative at neutral pH (Fig. 3). However, the quintuple mutant, Arch (DETC+V59A/P60L/P196S) (referred to as Arch-5) did show improved fluorescence at acidic pH over the parental mutations individually (Fig. 3) and was selected as a parent for another round of directed evolution.

Mutations V59A, P60L, D95E, and T99C in Arch-5 are predicted to be within 5 Å of the retinal Schiff-base linkage at K226 (the mutation P196S is predicted to be ∼13 Å away) (Fig. 4). To test whether the region surrounding the Schiff base contains other mutations that would increase fluorescence, we also constructed a dual site-saturation library at D222 and A225, the two binding-pocket residues closest to K226 not yet mutated in Arch-5 (Fig. 4), to explore all combinations of single and double mutations at these positions. We screened the library to 95% coverage (a total of 1,530 clones) at neutral pH. The variant with the most improved fluorescence over Arch-5 contained two additional mutations, D222S and A225C, and is referred to as Arch-7 (Fig. 3). Although Arch-7 showed improved overall fluorescence, it had reduced sensitivity to changes in pH (Fig. 3).

Evolved Arch Variants Have Improved Absolute Brightness in Vitro. In addition to Arch and Arch(DETC), we selected five laboratory-evolved Arch mutants for further biochemical analysis: [Arch (DETC + V59A), Arch(DETC + P60L), Arch(DETC + P196S), Arch-5, and Arch-7]. Arch(DETC) and the five evolved Arch mutants each have a red-shifted λ_{max} of 616–628 nm, or 60+ nm compared with wild-type Arch (Table 1 and Fig. S5), as well as fluorescence emission maxima at ∼730 nm (Table 1 and Fig. S6). All of the evolved variants we tested with improved fluorescence in live cells also have substantially improved quantum yields (Table 1). The brightest variants, Arch-5 and Arch-7, have quantum yields of 8.7×10^{-3} and 1.2×10^{-2}, respectively. Arch-7, therefore, is able to emit >1% of absorbed photons as fluorescence. Extinction coefficients were estimated with a hydroxylamine-mediated bleaching reaction (19) (Fig. S7). Although the range of quantum yields spans over an order of magnitude, the extinction coefficients lie in a much narrower range (Table 1). Arch-7 has the largest quantum yield, extinction coefficient, and, thus, absolute brightness of all tested Arch variants (Table 1). Spectrophotometric titrations of the transition between pigment-forming rhodopsin (protonated Schiff base) and near-UV absorbing rhodopsin (deprotonated Schiff base) as a function of pH were carried out (Fig. S8 and Table 1). The Schiff base of wild-type Arch has a $pK_a > 10$. Arch became unstable and irreversibly lost pigment in the pH range 10.6–11, indicative of denaturation. The Schiff-base pK_as of the Arch variants are significantly reduced with respect to wild-type Arch ($pK_a > 10$) and range from 6.85 to 8.44 (Table 1).

Live-Cell Imaging with Arch Variants. Because Arch is of interest for optogenetics applications in mammalian cells, we tested the ability of Arch(DETC) to express and fluoresce in a mammalian cell line. The D95E and T99C mutations were made in a mammalian codon-optimized version of Arch designed with golgi and endoplasmic reticulum export domains for enhanced membrane localization in mammalian neurons (20). Human embryonic kidney (HEK293) cells were transfected with the mammalian Arch and Arch(DETC) constructs and imaged following stimulation with a 633-nm laser. We found that Arch(DETC) had ∼4.5-fold improved fluorescence over Arch in HEK293 cells (Fig. 5). In *E. coli*, we did not detect any red fluorescence for wild-type Arch (using a different microscopy setup; see *SI Materials and Methods* for details) (Fig. 6). In contrast, far-red fluorescence from Arch-5 and Arch-7 was readily detectable in the membrane of single *E. coli* cells (Fig. 6). Arch-5 and Arch-7 also showed greatly improved fluorescence in *E. coli* over a published voltage-sensitive proteorhodopsin variant called PROPS (4) (Fig. S9).

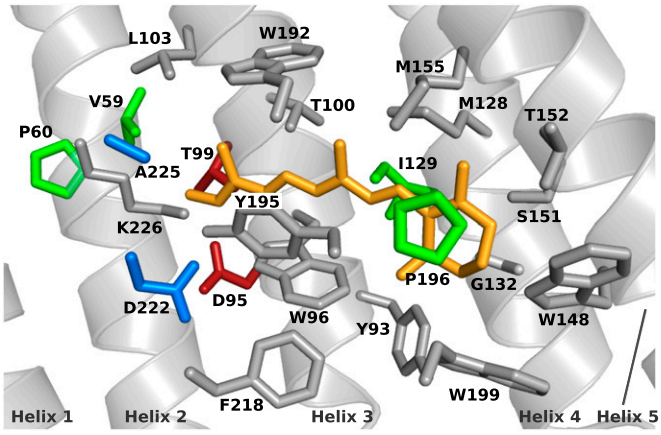

Fig. 4. Binding pocket of Arch according to a structural homology model based on AR-2. D95 and T99 are colored red. D222 and A225 are colored blue. Mutations from the error-prone library of Arch(DETC) that improved fluorescence are shown in green. The remaining residues within 5 Å of retinal are shown as gray sticks, and *all-trans* retinal is shown in orange.

Table 1. Biochemical characterization of purified Arch variants in 10 mM Tris, 200 mM NaCl, 0.15% DDM (pH 6.5)

Mutations	QY	ε, $M^{-1}{\cdot}cm^{-1}$	Brightness (QY × ε)/1,000	λ_{max}, nm	Max emission, nm	Stokes shift, nm	Schiff base, pK_a
Wild type	$1–9 \times 10^{-4}$*	64,828	<0.059	556	687*	131	>10
D95E, T99C	3.3×10^{-3}	38,436	0.12	626	731	103	7.5
D95E, T99C, P60L	4.0×10^{-3}	52,828	0.21	624	731	105	7.7
D95E, T99C, P196S	5.7×10^{-3}	44,116	0.22	628	731	105	6.8
D95E, T99C, V59A	6.2×10^{-3}	68,622	0.43	622	728	105	7.9
Arch-5: D95E, T99C, V59A, P60L, P196S	8.7×10^{-3}	65,126	0.57	622	731	107	7.6
Arch-7: D95E, T99C, V59A, P60L, P196S, D222S, A225C	1.2×10^{-2}	104,769	1.26	616	727	113	8.4

*Quantum yield (QY) of wild-type Arch has previously been reported to be 9×10^{-4} with maximum emission at 687 nm (3); due to its extreme dimness, we were not able to confidently measure the Arch emission spectrum in vitro (Fig. S6*A*). Using a fluorescence plate reader to collect Arch emission data, we estimated that the QY of Arch is closer to $\sim 1 \times 10^{-4}$.

Discussion

We used directed evolution to improve the quantum yield and absolute brightness of a rhodopsin, creating fluorescent integral membrane proteins suitable for general use in live-cell imaging and physiological sensing. Mutations that increased GR fluorescence could be transferred to the homologous residues in Arch to improve its overall fluorescence, despite GR and Arch sharing only a 26% amino acid sequence identity. And, although we used random mutagenesis to further improve Arch fluorescence, all of the confirmed beneficial mutations were very close to the retinal chromophore, indicating that fluorescence is sensitive to direct interactions between the chromophore and the protein. A recent spectroscopic analysis suggested that fluorescence of wild-type Arch is low but can be elevated through a sequential three-photon process where two consecutive quanta initialize formation of a highly fluorescent state Q formed from the photocycle intermediate N (18). An alternative approach is utilization of mutations of the Schiff-base counter ion (15) to increase the fluorescence yield in the initial (unphotolyzed) state. Although further study will be required to establish the biophysical role of specific mutations in improving Arch fluorescence, we expect that further improvements to fluorescence can be found by continued optimization of the retinal binding pocket.

Arch Variants Show Extreme Red-Shifted Fluorescence. The Arch mutants described here are the most red-shifted fluorescent proteins reported, with maximal emission at ~730 nm (and half-maximal emission at ~790 nm) (Fig. S6*B*), which is most probably caused by elimination or perturbation of the salt bridge between the negative charge of the counter ion and the protonated Schiff base (21) and elevation of the barrier in the excited state reaction pathway leading to isomerization. The red-shifted excitation/emission spectra mean that these Arch variants can be multiplexed with a variety of other fluorescent markers. Furthermore, they can likely be imaged deep into tissue due to their ability to be excited by light within the NIR window (22).

The laboratory-evolved Arch mutants described here have large Stokes shifts (differences between excitation and emission maxima) of >100 nm. Typical GFP-like proteins have very small Stokes shifts of 10–45 nm due to the rigidity of the chromophore within the protein matrix (23). The increased Stokes shift of Arch variants may be related to greater flexibility of the retinal chromophore within the protein structure. Large Stokes shifts are highly desirable in dual-color two-photon microscopy because two fluorescent markers can be excited with a single laser and then distinguished due to their well-separated emission maxima (24).

Comparison of Arch Variants with Other Fluorescent Proteins. Currently used fluorescent protein markers are based almost exclusively on *Aequorea victoria* GFP-like superfamily members, the most red-shifted of which emits maximally at 675 nm (23). Bacterial phytochrome receptors have recently emerged as potential substrates for the development of fluorescent markers in the NIR range (4, 13, 25). These proteins, which use biliverdin (an intermediate of heme metabolism) as a chromophore, can be engineered to excite and emit well into the infrared (termed iRFPs) (26). Recently a family of iRFP variants, iRFP640 to iRFP720, was reported to exhibit peak fluorescence emission between 670 nm and 720 nm, with excitation in the 643–702 nm range (25). Unlike members of the GFP-like superfamily and engineered bacterial phytochromes, however, Arch variants are not water-soluble and target fluorescence specifically to cellular membranes.

The brightest Arch variant identified in this study, Arch-7, with seven mutations in the retinal binding pocket, has a quantum yield between one and two orders of magnitude greater than that of wild-type Arch (the extreme dimness of Arch makes quantifying the exact improvement difficult) (Table 1 and Fig. S6*A*). While our manuscript was in review, an Arch variant containing five mutations (P60S, T80S, D95H, D106H, and F161V) was reported with quantum yield of 8×10^{-3} (1.5-fold less than Arch-7) (27). None of these individual mutations were identified in our evolution. T80 and F161 lie at the periphery of the protein, making it unlikely that mutations at these residues directly affect

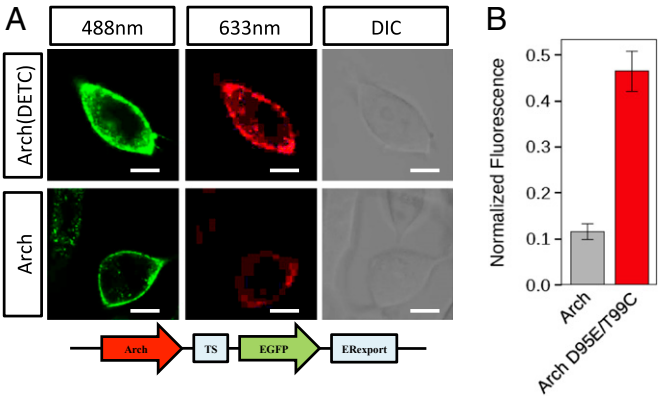

Fig. 5. Live-cell imaging of HEK293 cells expressing Arch and Arch(DETC) fused to EGFP. (*A*) HEK293 cells imaged following laser excitation at 488 nm or 633 nm. (Scale bars: 10 μm.) (*B*) Fluorescence of Arch and Arch(DETC) (12 cells each) normalized for total expression using the EGFP tag. Error-bars represent SEMs.

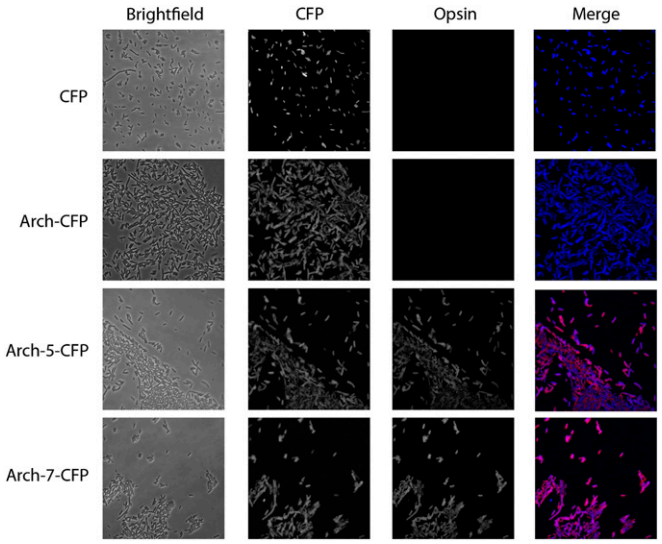

Fig. 6. Live-cell imaging of *E. coli* expressing translational fusions of wild-type Arch, Arch-5, or Arch-7 with CFP. *E. coli* expressing CFP alone are shown in the top row.

the protein's photo-physical properties (27). The absolute brightness of Arch-7, defined as the product of the extinction coefficient and quantum yield divided by 1,000, was determined to be 1.26 (Table 1). One of the brightest, most commonly used soluble red-shifted fluorescent proteins, mCherry (maximum excitation/emission = 587 nm/610 nm), has a brightness of 16, or 12.7-fold greater than that of Arch-7 (28). With a brightness value of 34, enhanced green fluorescent protein (eGFP; maximum excitation/emission = 488 nm/507 nm) is ∼27-fold brighter than Arch-7 (29, 30). The most red-shifted iRFP variant, iRFP720, which shows the most similar spectral characteristics to our evolved Arch variants of the published fluorescent proteins, has a brightness of 5.76 (∼4.6-fold great than Arch-7) (25). Thus, Arch-7 is significantly less bright than available soluble fluorescent proteins; however, to our knowledge, it is the brightest fluorescent integral membrane protein known. At cryogenic temperatures, bacteriorhodopsin reconstituted with a 13-*cis* acetylenic retinal analog exhibited a quantum efficiency close to 1 (31), suggesting that we may not have reached the physical–chemical limit for enhancing the fluorescence of these proteins. We believe improvements will be possible upon further directed evolution. Finally, the absorption maxima of fluorescent Arch variants reported here are significantly red-shifted compared with that of the wild-type protein (as are previously reported fluorescent GR variants) (15). Although the exact nature between the degree of red shift and fluorescence is not clear at this point, it would be interesting to investigate the effects on fluorescence of unnatural retinal analogs, which have been used previously to red-shift the λ_{max} of bacteriorhodopsin by hundreds of nanometers (32).

Potential Utility as Fluorescent pH/Voltage Indicators. The Schiff-base pK_a of Arch is >10, enabling light absorption in alkaline environments (Table 1). The fluorescent mutants presented here have pK_as that are significantly lower, thus resulting in loss of pigment at lower pH compared with wild-type Arch. The presence of retinal is required for fluorescence, and it is well documented that protonated Schiff base is required for pigment formation in the visible range (33); thus, the lower Schiff-base pK_a is most likely responsible for the observation of pH-sensitive fluorescence. Of the Arch mutants we characterized biochemically, Arch-7 had the highest Schiff-base pK_a of 8.44 (Table 1) and the least pH-sensitive fluorescence (between pH 5 and pH 9) of all of the tested mutants (Fig. 3). Arch(DETC+P196S) showed the most pH-sensitive fluorescence of the mutants we fully characterized and had the lowest Schiff-base pK_a (6.8) (Table 1).

E. coli is able to robustly buffer its cytosolic pH against changes in environmental pH up to pH ∼9 (34); in contrast, environmental pH can change drastically, and complex microenvironments such as biofilms can form distinct local heterogeneities in pH (35). A surface-displayed pH-sensitive GFP variant (pHluorin) was recently used to monitor pH changes surrounding *Streptococcus mutans* microcolonies during sucrose fermentation (36). We anticipate that fluorescent Arch variants expressed in *E. coli* (and perhaps other microorganisms) can also find use as "external" pH fluorescent indicators that can report on microenvironmental changes in pH in the far-red.

The reduced Schiff-base pK_a of Arch mutants also make them ideal candidates for voltage-sensing applications in neurons. Some of us recently showed that rat hippocampal neurons expressing Arch(DETC) in vitro exhibited improved fluorescence over those expressing wild-type Arch (while retaining fast kinetics), enabling optical detection of action potentials at lower laser intensity (37). Furthermore, Arch(DETC) expressed in the neurons of *Caenorhabditis elegans* exhibited odor-dependent changes in fluorescence, indicating that it can function as an optical readout of neuronal activity in these animals (37). Improved Arch fluorescence has important implications for the use of this sensor in live animals, surpassing the previous limitations of microbial rhodopsins' dim fluorescence in intact tissues. We envision the Arch variants described here to have broad applications as both physiological sensors and as genetically encoded fluorescent markers for labeling membranes in the far-red.

Materials and Methods

Plasmids and Bacterial Strains. Arch was obtained from genomic DNA of *Halorubrum sodomense* [strain 3755; German Collection of Microorganisms and Cell Cultures (DSMZ)]. Arch was amplified by PCR using the primers Arch_pET21a_FW and Arch_pet21a_REV (Table S1), which excluded the stop codon. The PCR product was cloned into the pET21a expression plasmid (EMD Millipore) between the NdeI and NotI restriction sites by isothermal assembly (38). This expression plasmid is referred to as pETME14. To construct a C-terminal fusion of Arch with CFP, pETME14 was linearized with XhoI and purified from a 1% agarose gel. CFP was PCR-amplified using primers with an overhang to linearized pETME14, and DNA fragments were assembled by isothermal assembly. Constructs were verified by sequencing (Laragen) using primers specific to the T7 promoter and terminator (Table S1). *E. cloni* EXPRESS BL-21(DE3) cells (Lucigen) were used for both cloning and expression of all Arch variants. Constructs were transformed into *E. coli* using the Gene Pulser Xcell Electroporation System (Bio-Rad Laboratories) in sterile 2-mm electroporation cuvettes with the following instrument settings: voltage = 2.5 kV, capacitance = 25 μF, resistance = 200 Ω.

Expression and Screening of Mutant Arch Libraries. Following transformation with library DNA, single colonies were picked with sterile toothpicks and inoculated into 200 μL of Luria broth (LB) supplemented with 100 μg/mL carbenicillin in deep-well 96-well plates. Plates were sealed with EasyApp Microporous Films (part no. 2977-6202; USA Scientific, Inc.), which facilitate air and gas exchange. Following overnight growth at 37 °C with shaking at 225 rpm and 80% humidity, the precultures were diluted 1:20 into 1 mL of fresh LB supplemented with 100 μg/mL carbenicillin and grown for 2 h at 30 °C. Then, 10 μM *all-trans* retinal and 500 μM isopropyl β-D-1 thiogalactopyranoside (IPTG) were then added to each well, and protein expression was allowed to continue for 4 h. Cells were pelleted at 4,500 × *g* in a swinging-bucket rotor, and the supernatant was decanted. Pellets were resuspended in 700 μL of 200 mM NaCl, and 180 μL of the resuspended cells was added to 20 μL of 500 mM potassium phosphate buffer (at pH 5, pH 7, or pH 9). Arch fluorescence was monitored in a Tecan plate reader at an emission wavelength of 720 nm following excitation at 620 nm. CFP fluorescence was monitored at an emission wavelength of 475 nm following excitation at 425 nm. The reported fluorescence is defined as A × (opsin fluorescence/CFP fluorescence) where A is an arbitrary scalar (set to 10,000). The reproducibility of opsin fluorescence measurements was confirmed by measuring the fluorescence of 87 different colonies expressing Arch(D95E/T99C)-CFP to compute a coefficient of variation of 8%.

Generation of Error-Prone PCR Library. Error-prone PCR reactions were carried out using reagents from the Taq PCR Core Kit (cat. no. 201223; Qiagen) according to the manufacturer's instructions with slight modifications. Three independent PCRs were carried out with 2× of each dNTP (400 μM) in the presence of 200 μM, 300 μM, or 400 μM $MnCl_2$, resulting in nucleotide error rates of 2.2, 4.36, and 5.6 per kilobase, respectively (Table S1, primers 5 and 6). PCR products were gel purified and cloned into Nde1/Not1-digested pETME14-eCFP using isothermal assembly. For error-prone PCR, thermocycler conditions were as follows: 2 min at 94 °C (1×); 30 s at 94 °C, 30 s at 55 °C, 1 min 15 s at 72 °C (35×); 10 min at 72 °C (1×). Libraries were independently transformed, and the retention of protein function (i.e., opsin fluorescence) was determined to be 83%, 53%, and 42% for the 200 μM, 300 μM, and 400 μM $MnCl_2$ library, respectively. Finally, 1,144 colonies from the 200-μM $MnCl_2$ library and 1,496 colonies from 300-μM $MnCl_2$ library were screened for increased fluorescence.

Generation of Site-Saturation Libraries. Site-saturation libraries were generated using a modified version of the QuikChange method (Stratagene), as previously described (15). For the single-site-saturation libraries, a mix of three mutagenic primers containing the triplet sequences NDT, VHG, and TGG were used in ratio of 12:9:1 for mutagenic PCR amplification (Table S1, primers 7–20). For the double-site-saturation library, a mixture of 9 mutagenic primers (and a reverse primer) was used for PCR amplification (Table S1, primers 21–30). This library design is referred to as the 22c-trick method (39). Library quality was confirmed by Sanger sequencing of 5–10 clones. Each library was screened from 95–98% coverage.

Arch Homology Model. An Arch homology model was produced based on the Archaerhodopsin II crystal structure (PDB ID code 1VGO, 86% protein sequence identity) using the SWISS-MODEL workspace (http://swissmodel.expasy.org/workspace/) (40, 41).

Purification of Arch Variants. *E. coli* were grown in LB supplemented with 100 μg/mL carbenicillin at 37 °C with 225 rpm shaking. Saturated overnight cultures were added to 1 L of fresh medium in large baffled flasks (2 L or 3 L total volume) and grown at 30 °C with 225 rpm shaking in the dark. When an OD_{600} of 0.5 was reached, cultures were supplemented with 10 μM *all-trans* retinal and 500 μM IPTG, and protein expression was allowed to continue for 4–6 h. Cells were pelleted at 4,500 × *g* and frozen at −20 °C overnight. Once frozen pellets were thawed at room temperature in the dark, 20 mL of extraction buffer (20 mM Tris, 200 mM NaCl, 3% (wt/vol) DDM, 1 mg/mL lysozyme, 0.1 mg/mL DNase I, pH 7.5) was added. Protein extraction continued for >30 min in the dark at room temperature, and cell suspensions were then spun at 20,000 × *g* at 4 °C. The supernatant was loaded onto a 1 mL His-tag purification column, and Arch variants were purified using an ÄKTA EXpress. Following purification, Arch variants were buffer exchanged into 10 mM Tris, 200 mM NaCl, 0.15% DDM (pH 6.5) exchanged using Amicon Ultra-15 centrifugal filters (part no. UFC801024; EMD Millipore), unless otherwise noted. A full description of methods used for biochemical characterization and live-cell imaging can be found in *SI Materials and Methods*.

ACKNOWLEDGMENTS. This work was funded by the Institute for Collaborative Biotechnologies through Grant W911NF-09-0001 from the US Army Research Office (to F.H.A.); National Institutes of Health (NIH) Grant 1R21MH103824-01 (to F.H.A. and V.G.); NIH Grant 1R01DA028299 (Massachusetts Institute of Technology sub-award 5710002669 to F.H.A.); NIH/National Institute of Neurological Disorders and Stroke New Innovator Award IDP20D017782-01 (to V.G.); NIH Grant GM29498 (to J.K.L. and S.P.B.); Division of Chemical Sciences, Geosciences, and Biosciences, Office of Basic Energy Sciences, Department of Energy Grant DEFG03-86ER13525 (to J.K.L. and S.P.B.); the German Research Foundation (M.K.M.E.) under Program EN 957/1-1; and California Institute of Technology (Caltech) Biology Division Training Grant NIH/NRSA 5T32GM07616 (to N.C.F.). V.G. acknowledges startup funds from the President and Provost of Caltech, the Biology and Biological Engineering Division of Caltech, and the Beckman Institute of Caltech. R.S.M. acknowledges financial support from the Shurl and Kay Curci Foundation and the Life Sciences Research Foundation.

1. Weissleder R (2001) A clearer vision for in vivo imaging. *Nat Biotechnol* 19(4):316–317.
2. Spudich JL, Jung KH (2005) Microbial rhodopsins: Phylogenetic and functional diversity. *Handbook of Photosensory Receptors*, eds Briggs WR, Spudich JL (Wiley, New York), pp 1–23.
3. Kralj JM, Douglass AD, Hochbaum DR, Maclaurin D, Cohen AE (2012) Optical recording of action potentials in mammalian neurons using a microbial rhodopsin. *Nat Methods* 9(1):90–95.
4. Kralj JM, Hochbaum DR, Douglass AD, Cohen AE (2011) Electrical spiking in Escherichia coli probed with a fluorescent voltage-indicating protein. *Science* 333(6040):345–348.
5. Berthold P, et al. (2008) Channelrhodopsin-1 initiates phototaxis and photophobic responses in chlamydomonas by immediate light-induced depolarization. *Plant Cell* 20(6):1665–1677.
6. Lozier RH, Bogomolni RA, Stoeckenius W (1975) Bacteriorhodopsin: A light-driven proton pump in Halobacterium Halobium. *Biophys J* 15(9):955–962.
7. Walter JM, Greenfield D, Liphardt J (2010) Potential of light-harvesting proton pumps for bioenergy applications. *Curr Opin Biotechnol* 21(3):265–270.
8. Gómez-Consarnau L, et al. (2010) Proteorhodopsin phototrophy promotes survival of marine bacteria during starvation. *PLoS Biol* 8(4):e1000358.
9. Nagel G, et al. (2005) Light activation of channelrhodopsin-2 in excitable cells of Caenorhabditis elegans triggers rapid behavioral responses. *Curr Biol* 15(24):2279–2284.
10. Berndt A, Lee SY, Ramakrishnan C, Deisseroth K (2014) Structure-guided transformation of channelrhodopsin into a light-activated chloride channel. *Science* 344(6182):420–424.
11. Kolodner P, Lukashev EP, Ching YC, Rousseau DL (1996) Electric-field-induced Schiff-base deprotonation in D85N mutant bacteriorhodopsin. *Proc Natl Acad Sci USA* 93(21):11618–11621.
12. Gong Y, Wagner MJ, Zhong Li J, Schnitzer MJ (2014) Imaging neural spiking in brain tissue using FRET-opsin protein voltage sensors. *Nat Commun* 5:3674.
13. Gong Y, Li JZ, Schnitzer MJ (2013) Enhanced Archaerhodopsin fluorescent protein voltage indicators. *PLoS ONE* 8(6):e66959.
14. Park J, et al. (2013) Screening fluorescent voltage indicators with spontaneously spiking HEK cells. *PLoS ONE* 8(12):e85221.
15. Engqvist MK, et al. (2014) Directed Evolution of Gloeobacter violaceus rhodopsin spectral properties. *J Mol Biol*, 10.1016/j.jmb.2014.06.015.
16. Song L, El-Sayed MA, Lanyi JK (1993) Protein catalysis of the retinal subpicosecond photoisomerization in the primary process of bacteriorhodopsin photosynthesis. *Science* 261(5123):891–894.
17. Balashov SP, et al. (2012) Aspartate-histidine interaction in the retinal schiff base counterion of the light-driven proton pump of Exiguobacterium sibiricum. *Biochemistry* 51(29):5748–5762.
18. Maclaurin D, Venkatachalam V, Lee H, Cohen AE (2013) Mechanism of voltage-sensitive fluorescence in a microbial rhodopsin. *Proc Natl Acad Sci USA* 110(15):5939–5944.
19. Wald G, Brown PK (1953) The molar extinction of rhodopsin. *J Gen Physiol* 37(2):189–200.
20. Gradinaru V, et al. (2010) Molecular and cellular approaches for diversifying and extending optogenetics. *Cell* 141(1):154–165.
21. Honig B, Ebrey T, Callender RH, Dinur U, Ottolenghi M (1979) Photoisomerization, energy storage, and charge separation: A model for light energy transduction in visual pigments and bacteriorhodopsin. *Proc Natl Acad Sci USA* 76(6):2503–2507.
22. Chu J, et al. (2014) Non-invasive intravital imaging of cellular differentiation with a bright red-excitable fluorescent protein. *Nat Methods* 11(5):572–578.
23. Piatkevich KD, et al. (2013) Extended Stokes shift in fluorescent proteins: Chromophore-protein interactions in a near-infrared TagRFP675 variant. *Sci Rep* 3:1847.
24. Tillo SE, Hughes TE, Makarov NS, Rebane A, Drobizhev M (2010) A new approach to dual-color two-photon microscopy with fluorescent proteins. *BMC Biotechnol* 10:6.
25. Shcherbakova DM, Verkhusha VV (2013) Near-infrared fluorescent proteins for multicolor in vivo imaging. *Nat Methods* 10(8):751–754.
26. Filonov GS, et al. (2011) Bright and stable near-infrared fluorescent protein for in vivo imaging. *Nat Biotechnol* 29(8):757–761.
27. Hochbaum DR, et al. (2014) All-optical electrophysiology in mammalian neurons using engineered microbial rhodopsins. *Nat Methods*, 10.1038/nmeth.3000.
28. Shaner NC, et al. (2004) Improved monomeric red, orange and yellow fluorescent proteins derived from Discosoma sp. red fluorescent protein. *Nat Biotechnol* 22(12):1567–1572.
29. Cormack BP, Valdivia RH, Falkow S (1996) FACS-optimized mutants of the green fluorescent protein (GFP). *Gene* 173(Spec No 1):33–38.
30. Kremers GJ, Gilbert SG, Cranfill PJ, Davidson MW, Piston DW (2011) Fluorescent proteins at a glance. *J Cell Sci* 124(Pt 2):157–160.
31. Balashov SP, et al. (1988) Light reactions and fluorescence of acetylenic analog of bacteriorhodopsin. *Molecular Physiology of Retinal Proteins*, ed Hara T (Yamada Science Foundation, Osaka, Japan), pp 345–346.
32. Asato AE, Li X-Y, Mead D, Patterson GML, Liu RSH (1990) Azulenic retinoids and the corresponding bacteriorhodopsin analogues: Unusually red-shifted pigments. *J Am Chem Soc* 112:7398–7399.
33. Sakmar TP, Franke RR, Khorana HG (1991) The role of the retinylidene Schiff base counterion in rhodopsin in determining wavelength absorbance and Schiff base pKa. *Proc Natl Acad Sci USA* 88(8):3079–3083.
34. Martinez KA, 2nd, et al. (2012) Cytoplasmic pH response to acid stress in individual cells of Escherichia coli and Bacillus subtilis observed by fluorescence ratio imaging microscopy. *Appl Environ Microbiol* 78(10):3706–3714.
35. Hidalgo G, et al. (2009) Functional tomographic fluorescence imaging of pH microenvironments in microbial biofilms by use of silica nanoparticle sensors. *Appl Environ Microbiol* 75(23):7426–7435.
36. Guo L, et al. (2013) investigating acid production by Streptococcus mutans with a surface-displayed pH-sensitive green fluorescent protein. *PLoS ONE* 8(2):e57182.
37. Flytzanis NC, et al. (2014) Archaerhodopsin variants with enhanced voltage sensitive fluorescence in mammalian and C. elegans neurons. *Nat Commun*, 10.1038/ncomms5894.
38. Gibson DG, et al. (2009) Enzymatic assembly of DNA molecules up to several hundred kilobases. *Nat Methods* 6(5):343–345.
39. Kille S, et al. (2013) Reducing codon redundancy and screening effort of combinatorial protein libraries created by saturation mutagenesis. *ACS Syn Biol* 2(2):83–92.
40. Bordoli L, et al. (2009) Protein structure homology modeling using SWISS-MODEL workspace. *Nat Protoc* 4(1):1–13.
41. Arnold K, Bordoli L, Kopp J, Schwede T (2006) The SWISS-MODEL workspace: A web-based environment for protein structure homology modelling. *Bioinformatics* 22(2):195–201.